Extraction of Network Parameters in The Electromagnetic Analysis of Planar Structures Using the Method of Moments

Mostafa N. Abdulla, *Student Member, IEEE*, and Michael B. Steer, *Fellow, IEEE*

Abstract—

Integration of electromagnetic and circuit analyses for the modeling of spatially distributed microwave and millimeter-wave circuits requires the establishment of ports which are defined in both the circuit and the electromagnetic realms. Four electromagnetic techniques are developed here and contrasted for the extraction of the port network parameters at circuit compatible ports. A full-wave method of moments electromagnetic analysis directly yielding network parameters of a slot–stripline-slot structure is formulated.

Keywords: method of moments, network characterization, field-circuit interaction, global modeling, and Green's functions.

I. Introduction

The Method of Moments (MoM) is an efficient way of electromagnetically modeling structures as pre-analysis, embedded in the Green's function, is used to reduce the numerical computation that would otherwise be required in more general techniques such as the Finite Element Method (FEM). This is especially true for antennas and open structures [1]. As sub-domain current basis functions and differential (or delta-gap) voltages are used in MoM formulation, the compatibility with general purpose microwave circuit simulators which use terminal current and voltage quantities is near optimum. However the interface thus defined is not compatible with the simulation of circuits. Several measurement-like electromagnetic (EM) techniques have been presented and shown to be well suited to extracting the scattering or circuit parameters of planar circuits [2]. These are classically deduced from the calculation of the surface current flowing on the structure [3]. This is analogous to slotted-line measurement of a standing-wave pattern and subsequent extraction of a one port reflection coefficient. Another approach implements a de-embedding procedure involving two through lengths of line to compensate for port discontinuities [4], a procedure very similar to that used in actual measurements. This de-embedding becomes increasingly complex when parameters at more than two ports are to be extracted as multiple "measurements" are required [5, 6]. Accuracy is improved by implementing matched terminations in the EM analysis using an integral equation technique as in [7] and [8], but more computations of the MoM matrix elements are involved. In MoM, basis functions of current are used and each, typically a rooftop or half rooftop function, straddles two geometric cells so that the coefficient of a basis function is the "differential-port" current flowing from one cell into its neighbor. The MoM formulation also uses the voltages between cells as variables and these are just differential-port voltages if the cells are not electrically connected (i.e. shorted in which case the voltage is zero). In structures with single layer metalization, the network parameters so extracted are referenced to the differential ports where active devices are placed and so can be used directly in circuit simulation [9–11]. The admittance parameter relationship between the currents and the voltages at the differential ports can be extracted from the inverted and reduced form of the MoM matrix (the procedure is described in [12–14]).

The situation is more complicated when a ground plane is involved as inevitably a port is defined with respect to the ground plane. This is because these ports are not differential ports but are referred to the ground plane (i.e. the voltage is referred to ground). Eleftheriades and Mosig [15] used a half basis function to define a port at the intersection of the walls of a shielded enclosure. This is an elegant procedure but not applicable in the absence of an enclosure (in open structures) or ports not at the walls of the enclosure but inside it. Building on the half basis function idea, Zhu *et al.* computed external port parameters for unbounded structures [16]. In [16], the authors use a segmentation approach to partition the feed lines from the rest of the circuit. In effect these feed lines are terminated in a virtual electrical wall and half basis functions are used. Then images of the lines are used to compute the inner port parameters. However this approach alters the physical behavior of a circuit in general. Introducing a vertical current element (basis function) in the position of a circuit port is, conceivably, one way of defining the inner circuit port in the MoM formulation. As an example of a more complicated situation, consider the problem of defining circuit ports for the extraction of the network parameters of a large open planar structure such as the slot-stripline-slot (SSS) spatial power combining amplifier shown in Fig. 1 [17, 18]. Each dimension of this system is around two wavelengths and is arranged as an $N \times N$ array of unit amplifiers. Each unit cell of the array is composed of an input stripline-coupled slot antenna, then a stripline mounted MMIC amplifier, and finally an output antenna,

This work was supported by the U.S. Army Research Office through Clemson University as a Multidisciplinary University Research Initiative on Quasi-Optical Power Combining, Agreement Number DAAG55-97-K-0132.

M. N. Abdulla is with Intel, 9750 Goethe Rd., LOC4/19, Sacramento, CA 95827-3500, USA, email: mnabdull@ieee.org.

M. B. Steer is with the Department of Electrical and Computer Engineering, North Carolina State University, Raleigh, NC27695-7914, USA, email: m.b.steer@ieee.org.

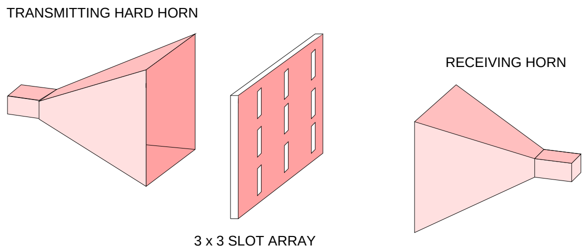

Fig. 1. A slot-stripline-slot spatial power combining system, showing a simplified 3×3 array.

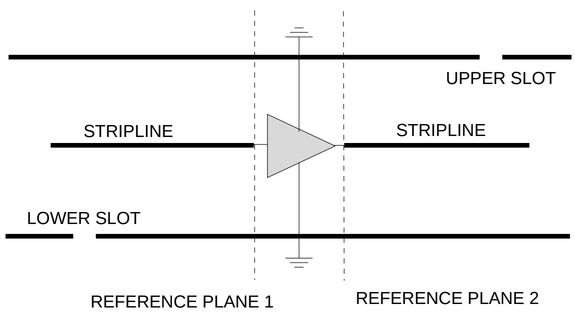

Fig. 2. Slot-stripline-slot (SSS) amplifier unit cell.

see Fig. 2.

The tight coupling of the antenna, circuit and (EM) environments requires global modeling of the entire, finite-sized structure and strategies for treating the EM model as an integral part of the circuit model [14, 19, 20].

The aim of the overall analysis is to develop a single network representation of the EM structure. The network is interfaced to circuit models at "electromagnetic terminals" defined to be consistent with nodal-based circuit descriptions. The depiction shown in Fig. 3 shows how the passive structure is reduced to an integrated model for a unit cell. In modeling an $N \times N$ array the two port network is replaced by a network with $2N^2$ ports and the input excitation is modeled using N equivalent sources at the input-side ports of the network. Each of the ports in Fig. 3 must be interfaced to the conventional circuit at normal

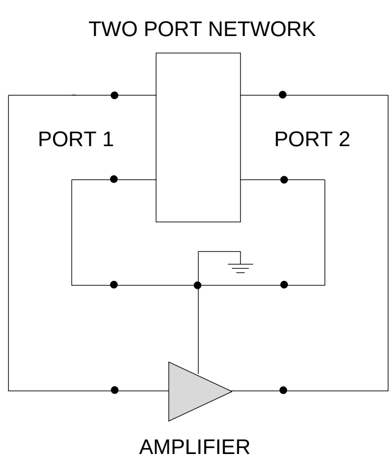

Fig. 3. Slot-stripline-slot (SSS) unit cell equivalent network.

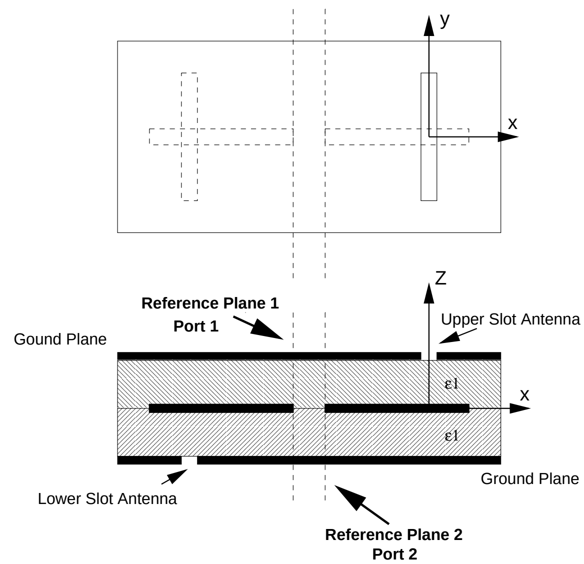

Fig. 4. Slot-stripline-slot (SSS) unit cell.

current/voltage defined terminals referenced to the ground planes. The terminals so referenced are called circuit ports whereas the ports immediately available from MoM analysis are differential ports [10, 11, 14]. The main contribution of this paper is the development and contrasting of a number of techniques for extracting the immittance parameters at circuit ports from the EM characterization at differential ports. Earlier work by our group relates these to the nodal parameters required by circuit simulators [9, 20]. Also a Mixed Potential Integral Equation (MPIE), implementing the ideas developed here, is developed for the full-wave analysis of SSS structure shown in Figs. 3 and 4 accounting for an incident EM field at the slot array.

II. Network Characterization

Without loss of generality consider the structure in Fig. 4. Circuit-compatibility requires that the parameters be referred to ports each of which has one terminal located on the stripline and the other located at the ground plane (assuming that the two ground planes are electrically identical). However only differential ports, with each port having two terminals located on either side of a break in the stripline is immediately available from EM analysis. In this section the four techniques illustrated in Fig. 5 are considered for translating the parameters extracted at the differential ports to parameters referred to the circuit ports. The first, Fig. 5(a), uses standard *standing wave characterization* determined by detecting the standing wave pattern on the line. Practically this is used only for characterizing one-port at a time and multiport characterization obtained using various impedance terminations at ports not being driven. However only one MoM matrix fill operation is required. The *stub de-embedding* technique, Fig. 5(b), is also used for one-port characterization, subsequently removing the impedance of the open circuit stub from the differential impedance to obtain the circuit port impedance. The third approach, Fig. 5(c), uses an open circuit *quarter*

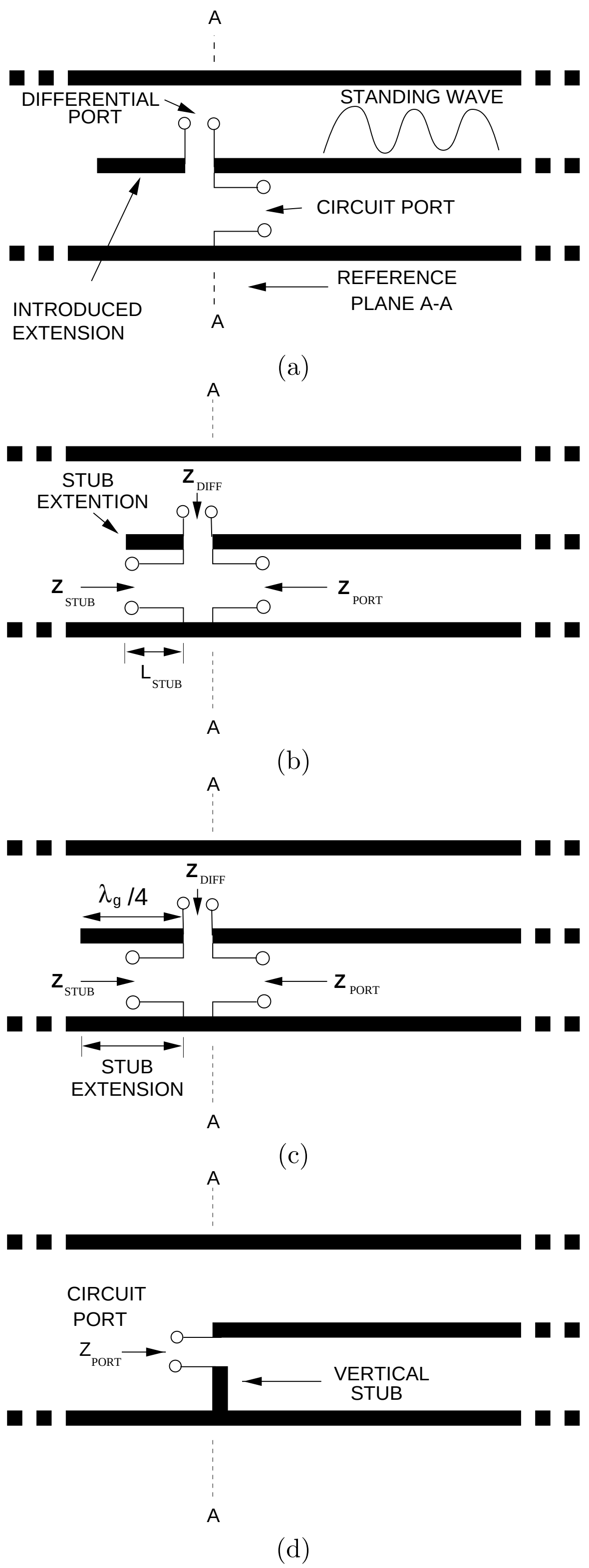

Fig. 5. Four techniques for establishing a circuit ports in MoM analysis: (a) standing wave characterization; (b) stub-de-embedding; (c) quarter wavelength stub; and (d) Vertical stub.

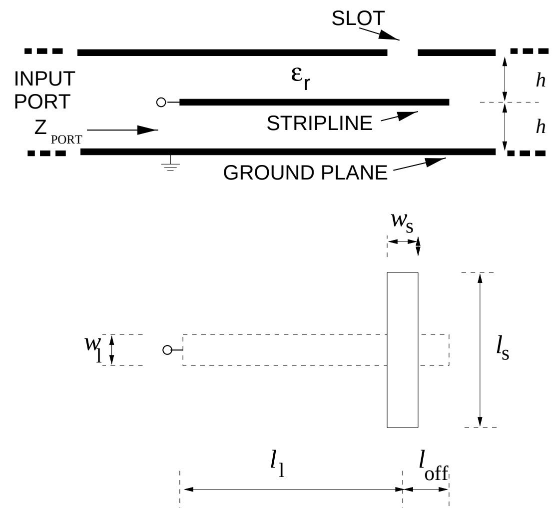

Fig. 6. Single port.

wavelength stub to present a short-circuit at one terminal of a differential port — thus transforming the differential port into the desired circuit port. In the final technique, Fig. 5(d), a *vertical stub* effectively introduces a conductor from the ground plane to the stripline so that the differential port between the wire and the stripline becomes the desired circuit port in the MoM formulation. The techniques are described in greater detail below in reference to the extraction of the input impedance, Z_{PORT}, of the simpler structure in Fig. 6.

A. Standing Wave Characterization

The *standing wave characterization* method mimics a laboratory measurement procedure as source is applied to a port and the standing wave pattern detected, see Fig. 5(a). Here a delta-gap source is introduced between two MoM cells at the differential port. The standing wave pattern enables the input reflection coefficient to be determined and referred to the desired reference plane. In this manner the discontinuity introduced by the source and the line extension do not affect the characterization. Multiport parameters are obtained by either exciting one port at a time and detecting the standing wave pattern at the other port, or by determining the input reflection coefficient at one port at a time with various loads at the other ports using a multiport extraction procedure [5, 6]. The number of permutations increases combinatorially as the number of ports increases. Generally an additional length of the line, at least one wavelength long, must be introduced between the excitation source and the reference plane to ensure TEM propagation where the standing wave pattern is detected. However, in some situations it may not be possible to insert such a long line because of the presence of other structures or the introduction of EM effects that were not present in the original structure. Fortunately, if the line can be inserted without interfering with the structure being model, coupling between the added line and the rest of the circuit can be excluded during matrix fill. A further problem with this method is that the characteristic impedance of

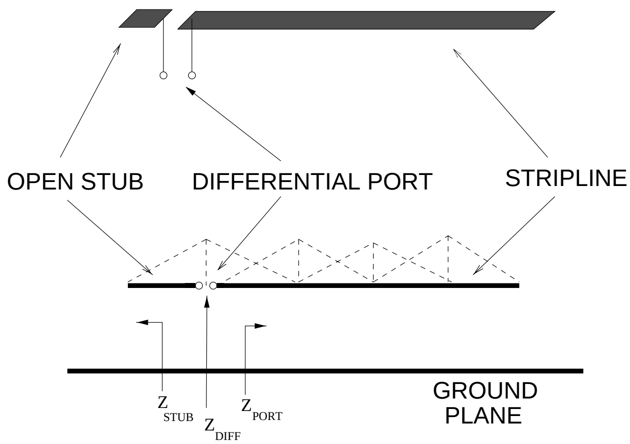

Fig. 7. Port definition for differential port and the differential bases cells.

the open stub must be determined separately.

B. Stub De-embedding

The stub de-embedding procedure is illustrated in Fig. 5(b). The input impedance calculated directly from MoM is the impedance Z_{DIFF} looking into the differential port which is the series combination of Z_{PORT} and the stub impedance Z_{STUB}, see Fig. 7, so that

$$Z_{PORT} = Z_{DIFF} - Z_{STUB} \tag{1}$$

$Z_{STUB} = Z_c \coth(\gamma L_{STUB})$ where the characteristic impedance Z_c and the propagation constant γ can be determined analytically or numerically.

For an N-port structure an $N\times N$ differential impedance matrix $\mathbf{Z}_{DIFF}$ can be extracted from the inverted and then reduced form of the MoM impedance matrix (the method is detailed in [14]). Then the $\mathbf{Z}_{PORT}$ matrix, also $N\times N$, is

$$\mathbf{Z}_{PORT} = \mathbf{Z}_{DIFF} - \mathbf{Z}_{STUB} \tag{2}$$

and $\mathbf{Z}_{STUB}$ is a diagonal matrix with elements $Z_{STUB,i}$, $i = 1, \cdots, N$ at the i th port. This method is computationally efficient as there is only one MoM matrix fill and solve. However the method does not account for fringing effects at the end of the stub nor possible non-TEM mode excitation on the stub and it increases the size of the MoM matrix. Also, as with the two port structure in Fig. 4, it is not always physically possible to insert the stub, even if it is of the minimum half basis function length.

C. Quarter-Wavelength Stub

If the stub of the previous technique is one quarter wavelength long, as in Fig. 5(c), $\mathbf{Z}_{PORT}$ can be calculated directly from the MoM as then $\mathbf{Z}_{STUB} = \mathbf{0}$ and so $\mathbf{Z}_{PORT} = \mathbf{Z}_{DIFF}$. The open circuit stub increases the MoM matrix size and has the same drawbacks as the previous method, but has the advantage that the characteristic impedance of the stub is not required. Note that the physical length of the stub must be changed with frequency. This approach is similar to that of Zhu *et al.* [16] who use images in a ground wall to create a short circuit.

D. Vertical Stub

The introduction of a vertical stub, as in Fig. 5(d), brings the ground reference up to the strip and forms a differential port which approximates the circuit port: $\mathbf{Z}_{PORT} \approx \mathbf{Z}_{DIFF}$. An appropriate basis function selections for one port are shown in Fig. 8. That is, a half rooftop basis function on the strip side of the port and pulse basis function on the vertical stub, both with current I^t, at the port terminals. The constraint imposed by I^t being the coefficient of two basis functions results in an expanded form of the MoM impedance matrix for an N port system:

$$\begin{bmatrix} \mathbf{Z}^{cc} & \mathbf{Z}^{ct} \\ \mathbf{Z}^{tc} & \mathbf{Z}^{tt} \end{bmatrix} \begin{bmatrix} \mathbf{I}^{c} \\ \mathbf{I}^{t} \end{bmatrix} = \begin{bmatrix} \mathbf{0} \\ \mathbf{V}^{t} \end{bmatrix} \tag{3}$$

where the superscript t denotes terminal quantities and the superscript c denotes quantities pertinent to currents induced on the conductor surface. I^c and I^t are the vectors of conductor and terminal current respectively. $\mathbf{Z}^{cc}$ in (3) is the MoM impedance matrix using the full rooftop basis functions. $\mathbf{V}^t$ is the vector of delta-gap voltage generators at the circuit ports and $\mathbf{I}^t$ is the vector of the port currents. The port admittance matrix $\mathbf{Y}^t$ (defined by $\mathbf{I}^t = \mathbf{Y}^t\mathbf{V}^t$) is obtained as follows: from (3)

$$\begin{bmatrix} \mathbf{I}^{c} \\ \mathbf{I}^{t} \end{bmatrix} = \begin{bmatrix} \mathbf{Z}^{cc} & \mathbf{Z}^{ct} \\ \mathbf{Z}^{tc} & \mathbf{Z}^{tt} \end{bmatrix}^{-1} \begin{bmatrix} \mathbf{0} \\ \mathbf{V}^{t} \end{bmatrix} \tag{4}$$

or

$$\begin{bmatrix} \mathbf{I}^{c} \\ \mathbf{I}^{t} \end{bmatrix} = \begin{bmatrix} \mathbf{Y}^{cc} & \mathbf{Y}^{ct} \\ \mathbf{Y}^{tc} & \mathbf{Y}^{tt} \end{bmatrix} \begin{bmatrix} \mathbf{0} \\ \mathbf{V}^{t} \end{bmatrix}. \tag{5}$$

Then (5), $\mathbf{Y}^t = \mathbf{Y}^{tt}$ which is the $N\times N$ submatrix in the lower right hand corner of the inverted impedance matrix in (4). This method introduces the smallest discontinuity and can be used with any multiport configuration in microstrip or stripline.

III. Structure Geometry and Modeling

The EM modeling of the SSS structure in Fig. 4 begins with the development of the Green's functions following the approach in [21] and using the MPIE and MoM techniques presented in [22] and [23]. First, using the equivalence principle [24], the center conductor at $z = 0$ in Fig. 4 is removed and replaced by an equivalent electric surface current density, J_s. Then the slot, at the $z = h$ plane, is removed and replaced by perfect electric conductors and the equivalent magnetic surface current density flowing at $z = h^-$ is

$$\mathbf{M}_s^{int} = \hat{z}\times\mathbf{E}_s \tag{6}$$

Finally, for the fields in the region $z > h$, the equivalent source is a magnetic surface current density flowing at $z > h^+$ and given by

$$\mathbf{M}_s^{ext} = -\mathbf{M}_s^{int} \tag{7}$$

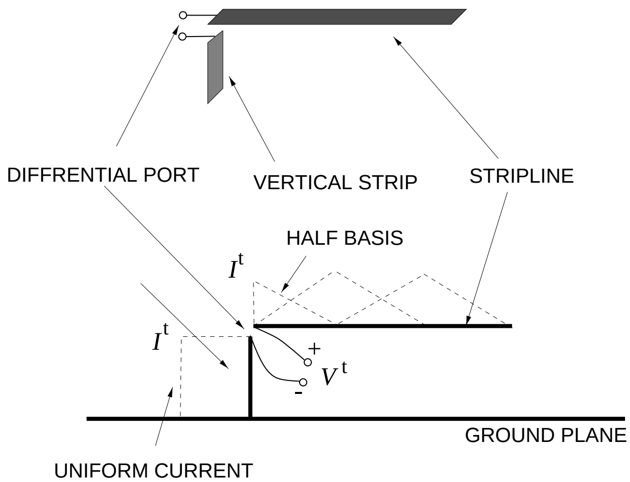

Fig. 8. Port definition for a unit cell using vertical current cell and half cell.

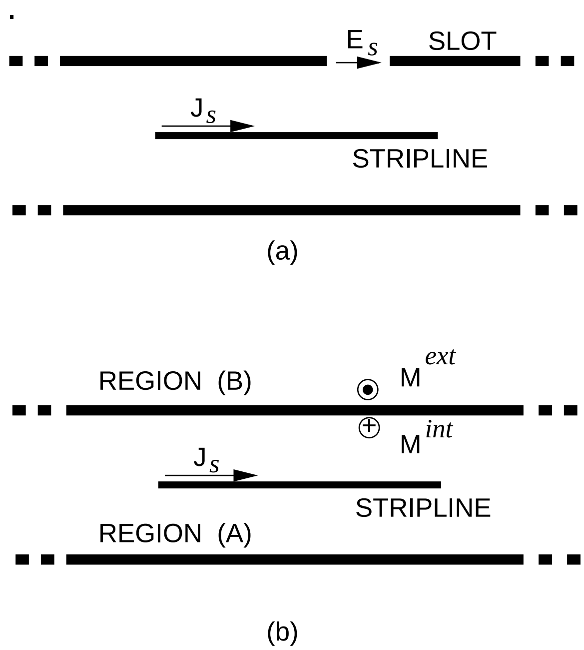

Fig. 9. Single slot-stripline-slot cell: (a) original structure; and (b) the structure after application of the equivalence principle.

The structure is thus decomposed into two regions as shown in Fig. 9 and the analysis reduces to determining the induced electric and magnetic surface current densities, $\mathbf{J}_s$, and $\mathbf{M}_s^{int}$. This is accomplished using MoM formulation which solves the MPIEs whose kernels are the Green's functions.

IV. Mixed Potential Integral Equations

In the internal region, region A in Fig. 9 (b), the electric and magnetic field distributions can be expressed as

$$\begin{aligned}\mathbf{E}^{int}(\mathbf{r}) &= \mathbf{E}_{inc}^{int}(\mathbf{r}) - j\omega\mathbf{A}^{int}(\mathbf{r}) - \nabla\phi^{int}(\mathbf{r}) \\ &\quad -\frac{1}{\epsilon}\nabla\times\mathbf{F}^{int}(\mathbf{r}), \qquad (8)\\ \mathbf{H}^{int}(\mathbf{r}) &= \mathbf{H}_{inc}^{int}(\mathbf{r}) - j\omega\mathbf{F}^{int}(\mathbf{r}) - \nabla\psi^{int}(\mathbf{r}) \\ &\quad +\frac{1}{\mu_0}\nabla\times\mathbf{A}^{int}(\mathbf{r}) \qquad (9)\end{aligned}$$

where $\mathbf{E}_{inc}^{int}(\mathbf{r})$ and $\mathbf{H}_{inc}^{int}(\mathbf{r})$ are the incident fields from the external excitation at the slots. $\mathbf{A}^{int}(\mathbf{r})$, $\mathbf{F}^{int}(\mathbf{r})$, $\phi^{int}(\mathbf{r})$, and $\psi^{int}(\mathbf{r})$ are the vector and scalar potentials of the electric and magnetic sources, respectively. In the external regions, regions B and C in Fig. 9(b), there are no electric sources, so that the electric and magnetic field distributions can be expressed as

$$\mathbf{E}^{ext}(\mathbf{r}) = \mathbf{E}_{inc}^{ext}(\mathbf{r}) - \frac{1}{\epsilon_0}\nabla\times\mathbf{F}^{ext}(\mathbf{r}), \qquad (10)$$

$$\mathbf{H}^{ext}(\mathbf{r}) = \mathbf{H}_{inc}^{ext}(\mathbf{r}) - j\omega\mathbf{F}^{ext}(\mathbf{r}) - \nabla\psi^{ext}(\mathbf{r}). \qquad (11)$$

Hence $\mathbf{E}_{inc}^{ext}(\mathbf{r})$ and $\mathbf{H}_{inc}^{ext}(\mathbf{r})$ are the field distributions of the incident waves from the external regions (B and C). $\mathbf{F}^{ext}(\mathbf{r})$ and $\psi^{ext}(\mathbf{r})$ are the vector and scalar potentials of the magnetic sources which are located immediately above the upper ground plane. Once the electric and magnetic field distributions are defined, the boundary conditions are enforced at both the stripline and the aperture. Since the tangential components of the electric field are zero on the stripline, the boundary condition is formulated as

$$\mathbf{E}^{int}(\mathbf{r}) = 0|_{\text{STRIPLINE}} \qquad (12)$$

Also the tangential components of the magnetic fields are continuous across the aperture so that

$$\mathbf{H}^{int}(\mathbf{r}) = \mathbf{H}^{ext}(\mathbf{r})|_{\text{APERTURE}} \qquad (13)$$

V. Green's Functions

The potentials of the electric and magnetic sources, $\mathbf{A}^{int}(\mathbf{r})$, $\mathbf{F}^{int}(\mathbf{r})$,$\mathbf{F}^{ext}(\mathbf{r})$, $\phi^{int}(\mathbf{r})$, $\psi^{int}(\mathbf{r})$, and $\psi^{ext}(\mathbf{r})$ can be represented as

$$\mathbf{A}^{int}(\mathbf{r}) = \int_{S_1} \overline{\overline{\mathbf{G}}}_A^{int}(\mathbf{r},\mathbf{r}')\cdot\mathbf{J}_s(\mathbf{r}')\,dS_1', \qquad (14)$$

$$\phi^{int}(\mathbf{r}) = \int_{S_1} G_\phi^{int}(\mathbf{r},\mathbf{r}')\;\rho_s(\mathbf{r}')\,dS_1', \qquad (15)$$

$$\mathbf{F}^{int}(\mathbf{r}) = \int_{S_2} \overline{\overline{\mathbf{G}}}_F^{int}(\mathbf{r},\mathbf{r}')\cdot\mathbf{M}_s(\mathbf{r}')\,dS_2', \qquad (16)$$

$$\psi^{int}(\mathbf{r}) = \int_{S_2} G_\psi^{int}(\mathbf{r},\mathbf{r}')\;\rho_{m_s}(\mathbf{r}')\,dS_2', \qquad (17)$$

$$\mathbf{F}^{ext}(\mathbf{r}) = \int_{S_2} \overline{\overline{\mathbf{G}}}_F^{ext}(\mathbf{r},\mathbf{r}')\cdot[-\mathbf{M}_s(\mathbf{r}')]dS_2', \qquad (18)$$

$$\psi^{ext}(\mathbf{r}) = \int_{S_2} G_\psi^{ext}(\mathbf{r},\mathbf{r}')\;[-\rho_{m_s}(\mathbf{r}')]dS_2'. \qquad (19)$$

where $\overline{\overline{\mathbf{G}}}_A^{int}(\mathbf{r},\mathbf{r}')$, $\overline{\overline{\mathbf{G}}}_F^{int}(\mathbf{r},\mathbf{r}')$, and $\overline{\overline{\mathbf{G}}}_F^{ext}(\mathbf{r},\mathbf{r}')$ are the spatial-domain dyadic Green's functions of vector potentials from the electric and magnetic currents in the internal and external regions (see the appendix). $G_\phi^{int}(\mathbf{r},\mathbf{r}')$, $G_\psi^{int}(\mathbf{r},\mathbf{r}')$, and $G_\psi^{ext}(\mathbf{r},\mathbf{r}')$ are the spatial-domain Green's functions of scalar potentials from the electric and magnetic charges in the internal and external regions, respectively(see the appendix). S_1 and S_2 represent the stripline

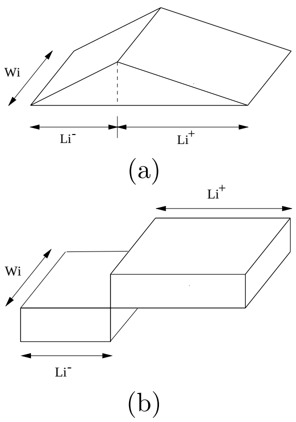

Fig. 10. Basis function: (a) rooftop and (b) pulse doublet.

and aperture surfaces, respectively. The quantities $\rho_s(\mathbf{r}')$ and $\rho_{m_s}(\mathbf{r}')$ are electric and magnetic charges and they are related to $\mathbf{J}_s(\mathbf{r}')$ and $\mathbf{M}_s(\mathbf{r}')$ by the continuity equations

$$\nabla.\mathbf{J_s} = -j\omega\rho_s, \quad (20)$$

$$\nabla.\mathbf{M_s} = -j\omega\rho_{m_s}. \quad (21)$$

VI. Method of Moments

The method of moments (MoM) formulation is developed by expanding and testing the MPIE using Galerkin's method to form a linear system of equations which is the MoM matrix set of equations. Assuming that the electric current density $\mathbf{J}_s$ flows in the x-direction and the magnetic current density $\mathbf{M}_s$ flows in the y-direction, then the electric and magnetic currents densities are expanded as

$$\mathbf{J}_s(\mathbf{r}) = \sum_{n=1}^{N} I_n T_n^x(\mathbf{r}), \quad (22)$$

$$\mathbf{M}_s(\mathbf{r}) = \sum_{m=1}^{M} V_m T_m^y(\mathbf{r}). \quad (23)$$

where T_n^x and T_m^y are rooftop basis functions as shown in Fig. 10(a). They are defined by

$$T_i^s(s) = \begin{cases} \frac{1+(s-s_i)/L_i}{W_i}, & s_i - L_i < s < s_i \\ \frac{1-(s-s_i)/L_i}{W_i}, & s_i < s < s_i + L_i \\ 0, & \text{otherwise} \end{cases} \quad (24)$$

where $s = x$ or y. The surface charge density is found using the continuity equation resulting in pulse doublets, see Fig. 10(b):

$$\Pi_i^s(s) = \begin{cases} \frac{-1}{L_i W_i}, & s_i - L_i < s < s_i \\ \frac{1}{L_i W_i}, & s_i < s < s_i + L_i \\ 0, & \text{otherwise} \end{cases} \quad (25)$$

where again $s = x$ or y. Upon introducing these distribution functions into the MPIEs and testing them with T_k^x, $k = 1$ to N, and T_l^y, $l = 1$ to M, the following system of integral equations is obtained:

$$\begin{aligned} \langle \mathbf{E}_{inc}^{int}, T_k^x \rangle &= j\omega\langle \mathbf{A}_t^{int}, \mathbf{T}_k \rangle + \langle (\nabla\phi^{int})_t, T_k^x \rangle \\ &\quad + \frac{1}{\epsilon}\langle (\nabla\times\mathbf{F}^{int})_t, T_k^x \rangle, \\ &\quad k = 1 \text{ to } N \qquad (26) \\ \langle (\mathbf{H}_{inc}^{int} - \mathbf{H}_{inc}^{ext})_t, T_l^y \rangle &= j\omega\langle (\mathbf{F}^{int} - \mathbf{F}^{ext})_t, T_l^y \rangle \\ &\quad + \langle (\nabla\psi^{int} - \nabla\psi^{int})_t, T_l^y \rangle \\ &\quad - \frac{1}{\mu_0}\langle (\nabla\times\mathbf{A}^{int})_t, T_l^y \rangle, \\ &\quad l = 1 \text{ to } M \qquad (27) \end{aligned}$$

where $\langle , \rangle$ specifies the inner product operation and the subscript t refers to the tangential components in the x-y plane. After reformulating the integral equations above, the matrix equation

$$\begin{bmatrix} \langle \Delta H^{inc}, T_l^y \rangle \\ \langle E_s{}^{inc}, T_k^x \rangle \end{bmatrix} = \begin{bmatrix} \mathbf{Y} & \mathbf{U} \\ \mathbf{W} & \mathbf{Z} \end{bmatrix} \begin{bmatrix} \mathbf{V} \\ \mathbf{I} \end{bmatrix} \quad (28)$$

is obtained. $\mathbf{Y}_{M\times M}$ is the self-coupling submatrix of the slot; $\mathbf{Z}_{N\times N}$ is the self-coupling submatrices of the stripline; $\mathbf{U}_{M\times N}$ is the coupling submatrix between the slot and the stripline; and $\mathbf{W}_{N\times M}$ is the coupling submatrix between the stripline and the slot. The vectors, $\mathbf{V}_{M\times 1}$, and $\mathbf{I}_{N\times 1}$ are the unknown coefficients of the basis functions on the slot, and stripline respectively. Finally, this matrix is composed of submatrices with each describing the interaction of two regions of the equivalent model in Fig. 9(b). $\left[\langle \Delta H^{inc}, T_l^y \rangle\right]_{M\times 1}$, $\left[\langle E^{inc}, T_k^x \rangle\right]_{N\times 1}$ are the excitation vectors from the incident fields.

The MoM matrix in (28) is further partitioned two ways: an internal region matrix, and an external region matrix. Here the Green's functions of the external and internal regions are calculated separately and they depend on the cascading structures [25]. The matrix in (28) is therefore calculated as

$$\begin{bmatrix} \mathbf{Y} & \mathbf{U} \\ \mathbf{W} & \mathbf{Z} \end{bmatrix} = \begin{bmatrix} \mathbf{Y}^{ext} & \mathbf{0} \\ \mathbf{0} & \mathbf{0} \end{bmatrix} + \begin{bmatrix} \mathbf{Y}^{int} & \mathbf{U}^{int} \\ \mathbf{W}^{int} & \mathbf{Z}^{int} \end{bmatrix} \quad (29)$$

where $\mathbf{Y}^{ext}$ is the mutual coupling integrals for the external region and $\mathbf{Y}^{int}$, $\mathbf{U}^{int}$, $\mathbf{W}^{int}$, and $\mathbf{Z}^{int}$ are the mutual coupling for the closed array structure with ji elements

$$\begin{aligned} Z_{ji}^{int} &= j\omega\langle (\mathbf{A}_{ji}^{int})_t, T_j^x \rangle + \langle (\nabla\phi_{ji}^{int})_t, T_j^x \rangle, \\ &= j\omega \int_{y_j-\frac{W_j}{2}}^{y_j+\frac{W_j}{2}} \int_{x_j-L_j}^{x_j+L_j} \int_{y_i-\frac{W_i}{2}}^{y_i+\frac{W_i}{2}} \int_{x_i-L_i}^{x_i+L_i} \\ &\quad T_j^x(x)\, G_{A_{xx}}^{int}(x|x';y|y';0|0)\, T_i^x(x')\, dx'dy'dx\,dy \\ &\quad - \frac{1}{j\omega} \int_{y_j-\frac{W_j}{2}}^{y_j+\frac{W_j}{2}} \int_{x_j-L_j}^{x_j+L_j} \int_{y_i-\frac{W_i}{2}}^{y_i+\frac{W_i}{2}} \int_{x_i-L_i}^{x_i+L_i} \\ &\quad \Pi_j^x(x)\, G_\phi^{int}(x|x';y|y';0|0)\, \Pi_i^x(x')\, dx'dy'dx\,dy, \end{aligned} \quad (30)$$

$$Y_{ji}^{int} = j\omega\langle (\mathbf{F}_{ji}^{int})_t, T_j^y \rangle + \langle (\nabla\psi_{ji}^{int})_t, T_j^y \rangle$$

$$\begin{aligned} &= j\omega \int_{x_j-\frac{W_j}{2}}^{x_j+\frac{W_j}{2}} \int_{y_j-\frac{W_i}{2}L_j}^{y_j+L_j} \int_{x_i-\frac{W_i}{2}}^{x_i+\frac{W_i}{2}} \int_{y_i-L_i}^{y_i+L_i} \\ &\quad T_j^y(y)\, G_{F_{yy}}^{int}(x|x';y|y';h|h)\, T_i^y(y')\; dx'dy'dx\,dy \\ &\quad -\frac{1}{j\omega} \int_{x_j-\frac{W_j}{2}}^{x_j+\frac{W_j}{2}} \int_{y_j-L_j}^{y_j+L_j} \int_{x_i-\frac{W_i}{2}}^{x_i+\frac{W_i}{2}} \int_{y_i-L_i}^{y_i+L_i} \\ &\quad \Pi_j^y(y)\, G_{\psi}^{int}(x|x';y|y';h|h)\, \Pi_i^y(y')\; dx'dy'dx\,dy, \end{aligned} \quad (31)$$

$$\begin{aligned} Y_{ji}^{ext} &= j\omega\langle(\mathbf{F}_{ji}^{ext})_t, T_j^y\rangle + \langle(\nabla\psi_{ji}^{ext})_t, T_j^y\rangle \\ &= j\omega \int_{x_j-\frac{W_j}{2}}^{x_j+\frac{W_j}{2}} \int_{y_j-L_j}^{y_j+L_j} \int_{x_i-\frac{W_i}{2}}^{x_i+\frac{W_i}{2}} \int_{y_i-L_i}^{y_i+L_i} \\ &\quad T_j^y(y)\, G_{F_{yy}}^{ext}(x|x';y|y';h|h)\, T_i^y(y')\; dx'dy'dx\,dy \\ &\quad -\frac{1}{j\omega} \int_{x_j-\frac{W_j}{2}}^{x_j+\frac{W_j}{2}} \int_{y_j-L_j}^{y_j+L_j} \int_{x_i-\frac{W_i}{2}}^{x_i+\frac{W_i}{2}} \int_{y_i-L_i}^{y_i+L_i} \\ &\quad \Pi_j^y(y)\, G_{\psi}^{ext}(x|x';y|y';h|h)\, \Pi_i^y(y')\; dx'dy'dx\,dy, \end{aligned} \quad (32)$$

$$\begin{aligned} W_{ji}^{int} &= \frac{1}{\epsilon}\langle(\nabla\times\mathbf{F}_{ji}^{int})_t, T_j^x\rangle \\ &= \frac{1}{\epsilon} \int_{x_j-\frac{W_j}{2}}^{x_j+\frac{W_j}{2}} \int_{y_j-L_j}^{y_j+L_j} \int_{y_i-\frac{W_i}{2}}^{y_i+\frac{W_i}{2}} \int_{x_i-L_i}^{x_i+L_i} \\ &\quad T_j^y(x)\, [\frac{\partial}{\partial z} G_{F_{yy}}^{int}(r|r')]|_{z=0,z'=h} T_i^x(y') \\ &\qquad dx'dy'dx\,dy, \end{aligned} \quad (33)$$

$$\begin{aligned} U_{ji}^{int} &= -\frac{1}{\mu_0}\langle(\nabla\times\mathbf{A}_{ji}^{int})_t, T_j^y\rangle \\ &= -\frac{1}{\mu_0} \int_{y_j-\frac{W_j}{2}}^{y_j+\frac{W_j}{2}} \int_{x_j-L_j}^{x_j+L_j} \int_{x_i-\frac{W_i}{2}}^{x_i+\frac{W_i}{2}} \int_{y_i-L_i}^{y_i+L_i} \\ &\quad T_j^x(x)\, [\frac{\partial}{\partial z} G_{A_{xx}}^{int}(r|r')]|_{z=h,z'=0} T_i^y(y') \\ &\qquad dx'dy'dx\,dy. \end{aligned} \quad (34)$$

With the vertical stub a half basis function is used at the end of the stripline and the coefficient of this basis function is the port current. Assuming that the vertical strip is electrically thin, we can assume that the current at the half basis equals the vertical current (see Fig. 8). Thus the half basis function is referred to as a port basis. As denoted in (3), the interactions between port-basis (half basis) and the regular basis elements, which are represented by the $\mathbf{Z}^{ct}$ and $\mathbf{Z}^{tc}$ submatrices, are

$$\begin{aligned} Z_{ji}^{ct} &= j\omega \int_{y_j-\frac{W_j}{2}}^{y_j+\frac{W_j}{2}} \int_{x_j-L_j}^{x_j+L_j} \int_{y_i-\frac{W_i}{2}}^{y_i+\frac{W_i}{2}} \int_{x_i}^{x_i+L_i} \\ &\quad T_j^x(x)\, {G_{A_{xx}}}^{int}(x|x';y|y';0|0)\, T_i^x(x')\; dx'dy'dx\,dy \\ &\quad -\frac{1}{j\omega} \int_{y_j-\frac{W_j}{2}}^{y_j+\frac{W_j}{2}} \int_{x_j-L_j}^{x_j+L_j} \int_{y_i-\frac{W_i}{2}}^{y_i+\frac{W_i}{2}} \int_{x_i}^{x_i+L_i} \\ &\quad \Pi_j^x(x)\, G_{\phi}^{int}(x|x';y|y';0|0)\, \Pi_i^x(x')\; dx'dy'dx\,dy, \end{aligned} \quad (35)$$

$$\begin{aligned} Z_{ji}^{tc} &= j\omega \int_{y_j-\frac{W_j}{2}}^{y_j+\frac{W_j}{2}} \int_{x_j}^{x_j+L_j} \int_{y_i-\frac{W_i}{2}}^{y_i+\frac{W_i}{2}} \int_{x_i-L_i}^{x_i+L_i} \\ &\quad T_j^x(x)\, {G_{A_{xx}}}^{int}(x|x';y|y';0|0)\, T_i^x(x')\; dx'dy'dx\,dy \\ &\quad -\frac{1}{j\omega} \int_{y_j-\frac{W_j}{2}}^{y_j+\frac{W_j}{2}} \int_{x_j}^{x_j+L_j} \int_{y_i-\frac{W_i}{2}}^{y_i+\frac{W_i}{2}} \int_{x_i-L_i}^{x_i+L_i} \\ &\quad \Pi_j^x(x)\, G_{\phi}^{int}(x|x';y|y';0|0)\, \Pi_i^x(x')\; dx'dy'dx\,dy. \end{aligned} \quad (36)$$

The transverse fields generated by the vertical current is described by elements

$$\begin{aligned} Z_{ji}^{xz} &= j\omega \int_{y_j-\frac{W_j}{2}}^{y_j+\frac{W_j}{2}} \int_{x_j-L_j}^{x_j+L_j} \int_{y_i-\frac{W_i}{2}}^{y_i+\frac{W_i}{2}} \int_{-h}^{0} \\ &\quad T_j^x(x)\, {G_{A_{xz}}}^{int}(x|x';y|y';0|z')\; dz'dy'dx\,dy \\ &\quad -\frac{1}{j\omega} \int_{y_j-\frac{W_j}{2}}^{y_j+\frac{W_j}{2}} \int_{x_j-L_j}^{x_j+L_j} \int_{y_i-\frac{W_i}{2}}^{y_i+\frac{W_i}{2}} \int_{h}^{x_i+L_i} \\ &\quad \Pi_j^x(x)\, G_{\phi}^{int}(x|x';y|y';0|z')\, \delta(z')\; dz'dy'dx\,dy. \end{aligned} \quad (37)$$

VII. Results

To illustrate the difference between the differential and circuit port characterization consider the strip coupled slot antenna in Fig. 6 with $l_L = 50$ mm, $W_L = 2.5$ mm, $l_S = 30$ mm, $W_S = 2$ mm, $l_{OFF} = 10$ mm, $h = 1.57$ mm, and $\epsilon_r = 2.2$. Details of the structure that is being used in developing the characterization is shown in Fig. 7 where the added open stub is 3 mm long. In Fig 11 the reflection coefficient Γ_{DIFF} (corresponding to Z_{DIFF}) is compared to the reflection coefficient Γ_{PORT} (corresponding to Z_{PORT}) extracted using stub de-embedding method. The propagation constant and characteristic impedance were determined analytically. Not surprisingly there is a significant discrepancy between the port and the differential parameters. A problem with both stub de-embedding methods is accounting for the fringing at the open circuited stub. With both de-embedding methods the end of the stub was considered to be an open circuit. The error involved in this and the imprecision inherent in characterizing the transmission line (i.e. determining Z_c and γ) are responsible for the small discrepancy between the two procedures.

The central aim of this paper is to contrast the four differential characterization procedures. The quarter wavelength stub de-embedding procedure has already been contrasted above and will not be considered further as the long additional variable length of the stub is problematic. The real and imaginary components of Z_{PORT} for the stripline coupled slot antenna are presented in Figs. 12 and 13 using standing wave characterization, sub de-embedding and vertical stub methods. The three methods yield consistent characterizations. The standing wave and vertical stub methods methods yield almost identical resistive characterization, see Fig. 12. The three methods show larger variation when the port reactance is considered, see Fig. 13. This is attributed to energy storage (i.e. reactance)

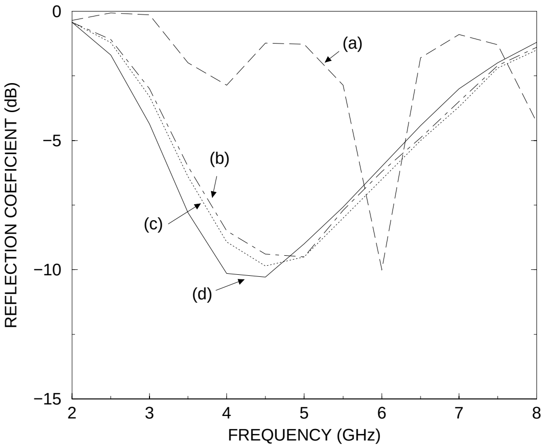

Fig. 11. Return loss of a single slot antenna using: (a)Z_{DIFF}; (b)Z_{PORT} extracted using stub de-embedding; and (c) Z_{PORT} after [23]. Referring to 6 $l_L = 50mm$, $W_L = 2.5mm$, $l_S = 30mm$, $W_S = 2mm$, $l_{OFF} = 10mm$,$h = 1.57mm$, and $\epsilon_r = 2.2$.

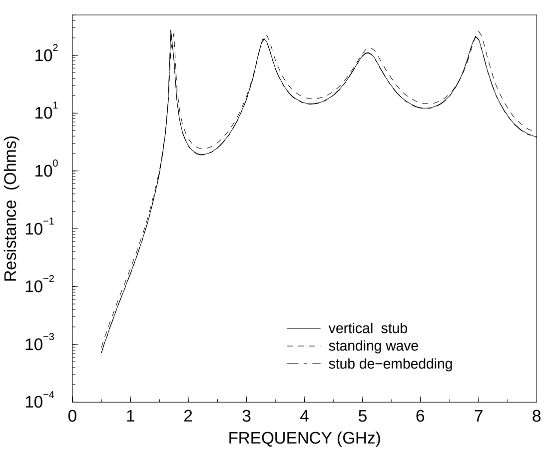

Fig. 12. Resistance of single slot circuit.

associated with the open stubs and the modification of the EM fields (again a reactive effect) caused by the vertical stub. The inductive effect of the stub should be accounted for. In the work we are undertaking this is incorporated in the model of the active devices connected to the distributed network.

VIII. Discussion

This paper dealt with the port definition required to interface circuit and EM analyses. The method of moments EM analysis applied to structures with ground plane, with appropriately chosen current basis functions, yields network characterization at differential ports. In this paper four techniques were constructed for transforming this characterization into the desired circuit port characterization. The techniques were all comparable and differ in

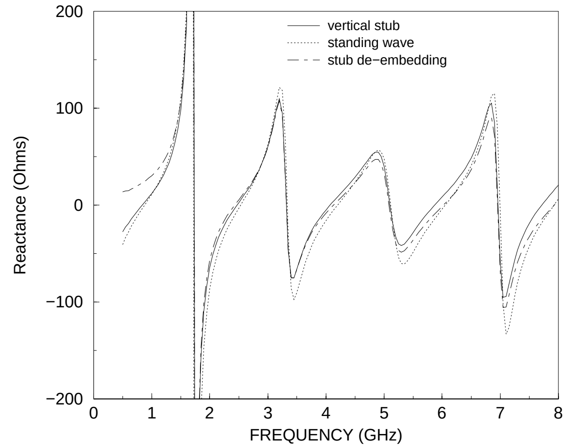

Fig. 13. Reactance of single slot circuit.

terms of the additional structures required, affect on MoM matrix size, and ease of implementation. With all of these considerations the vertical stub method is preferred but it results in greater complexity in developing the Green's functions behind MoM analysis. Another contribution of this paper was the development of the MoM electromagnetic analysis for a three layer slot-stripline-slot structure.

References

[1] T. Itoh, *Numerical Techniques for Microwave and Millimeter-Wave Passive Structures*, John Wiley & Sons, Inc., New York, 1989.

[2] L. P. Dunleavy and P. B. Katehi, "A generalized method for analyzing shielded thin microstrip discontinuities," *IEEE Trans. Microwave Theory Tech*, vol. 36, Dec. 1988, pp. 1758–1766.

[3] P. B. Katehi and N. Alexopoulos, "On the modeling of electromagnetically coupled microstrip antennas—the printed dipole," *IEEE Trans. Antennas and Propagat.*, vol. 32, Dec. 1984, pp. 116–118.

[4] J. C. Rautio, "A new definition of characteristic impedance," *1991 IEEE MTT-S Int. Microwave Symp. Digest*, June 1991, pp. 761–764.

[5] S. B. Goldberg, M. B. Steer, P. D. Franzon and J. S. Kasten, "Experimental electrical characterization of interconnects and discontinuities in high speed digital systems," *IEEE Trans. on Components Hybrids and Manufacturing Technology*, vol. 14, Dec. 1991, pp. 761–765.

[6] S. B. Goldberg, M. B. Steer and P. D. Franzon, "Accurate experimental characterization of three-ports," 1991 *IEEE MTT-S Int. Microwave Symp. Digest*, June 1991, pp. 241-244.

[7] R. Gillard, J. H. Corre, M. Drissi and J. Citerne, "A general treatment of matched terminations using integral equations modeling and application," *IEEE Trans. Microwave Theory Tech.*, vol. 42, Dec. 1994, pp. 2545–2553.

[8] E. K. L. Yeung, J. C. Beal, and Y. M. M Antar, "Matched load simulation for multiport microstrip structures," *Electronic Let.*, vol. 29, May 1993, pp. 867-868.

[9] C. E. Christoffersen and M. B. Steer, "Implementation of the local reference node concept for spatially distributed circuits," *Int. J. on RF and Microwave Computer Aided Engineering*, vol. 9, No. 4, 1999. In Press

[10] C. E. Christoffersen, M. A. Summers and M. B. Steer, "Harmonic balance analysis for systems with circuit-field interaction," *1998 IEEE MTT-S Int. Microwave Symp. Digest*, June 1998, pp. 1131–1134.

[11] T. W. Nuteson, G. P. Monahan, M. B. Steer, K. Naishadham, J. W. Mink, K. Kojucharoff and J. Harvey, "Full-wave analy-

sis of quasi-optical structures," *IEEE Trans. Microwave Theory Tech.*, vol. 44, May 1996, pp. 701–710.
[12] M. N. Abdulla, U. A. Mughal and M. B. Steer, "Network characterization of a finite array of folded-slot antennas for spatial power combining application," *Proc. IEEE Antenna and Propagation Symp.*, July, 1999.
[13] M. N. Abdulla, U. A. Mughal, H.-S. Tsai, M. B. Steer and R. A. York, "A full-wave system simulation of a folded-slot spatial power combining amplifier array," *1999 IEEE MTT-S Int. Microwave Symp. Digest*, June 1999.
[14] M. B. Steer, J. F. Harvey, J. W. Mink, M. N. Abdulla, C. E. Christoffersen, H. M. Gutierrez, P. L. Heron, C. W. Hicks, A. I. Khalil, U. A. Mughal, S. Nakazawa, T. W. Nuteson, J. Patwardhan, S. G. Skaggs, M. A. Summers, S. Wang and A. B. Yakovlev, "Global modeling of spatially distributed millimeter-wave systems," *IEEE Trans. Microwave Theory Tech.*, vol. 47, June 1999.
[15] G. V. Eleftheriades and J. R. Mosig, "On the network characterization of planar passive circuits using the method of moments," *IEEE Trans. Microwave Theory Tech*, Mar. 1996, pp. 438–445.
[16] L. Zhu and K. Wu, "Characterization of unbounded multiport microstrip passive circuit using an explicit network-based method of moments," *IEEE Trans. Microwave Theory Tech.*, vol. 45, Dec. 1997, pp. 2114–2124.
[17] J. Hubert, J. Schoenberg and Z. B. Popović, "High-power hybrid quasi-optical Ka-band amplifier design," *1995 IEEE MTT-S Int. Microwave Symp. Digest*, vol. 2, June 1995, pp. 585-588.
[18] R. A. York and Z. B. Popović, *Active and quasi-optical arrays for solid-state power combining,* John Wiley & Sons, Inc., 1997.
[19] M. N. Abdulla and M. B. Steer, "A partitioning approach to large scale electromagnetic problems applied to an array of microstrip coupled slot antennas," *1998 IEEE MTT-S Int. Microwave Symp. Digest*, June 1998, pp. 1783–1786.
[20] A. I. Khalil and M. B. Steer, "Circuit theory for spatially distributed microwave circuits," *IEEE Trans. Microwave Theory Tech.*, vol. 46, Oct. 1998, pp. 1500–1503.
[21] P. S. Simon, K. McInturff, D. L. Johnson, and J. A. Troychak, "Moment method analysis of a strip-fed finite slot using subdomain basis function,"*1989 Antenna Application Symp. Digest*, Sept. 1989, pp. 477–505.
[22] C. Chen and N. G. Alexopoulos, "Radiation by aperture antennas of arbitrary shape fed by a covered microstrip line," *Proc. IEEE Antenna and Propagation Symp.*, 1993, pp. 438–445.
[23] C. Chen, W. E. McKinzie and N. G. Alexopoulos, "Strip-fed arbitrarily shaped printed-aperture antennas," *IEEE Trans. Antenna and Propagation*, vol. 45, July 1997, pp. 1186–1198.
[24] R. F. Harrington, *Field Computation by Moment Methods*, Macmillan, New York, 1968.
[25] M. N. Abdulla and M. B. Steer, "A finite double-layer slot array structure for spatial power combining amplifier," *Proc. IEEE Antennas and Propagation Symp.*, 1998, pp. 1206–1209.

IX. Appendix

A. Internal Region Green's Functions

The Green's functions of the region between the outer conductive layers, see Fig. 9, are described by G_d, a Dirichlet Green's function, and G_n, a Neumann Green's function, both of which are the solution of

$$\left(\nabla^2 + k^2\right) G_{d,n}\left(\mathbf{r},\mathbf{r}'\right) = -\delta\left(\mathbf{r},\mathbf{r}'\right) \tag{38}$$

and satisfy either Dirichlet or Neumann boundary conditions at the parallel plates. The boundary conditions of the potentials on the perfect conductor are

$$\phi = 0, \tag{39}$$
$$\frac{\partial\psi}{\partial n} = 0, \tag{40}$$
$$\hat{n}\times\mathbf{A} = 0, \tag{41}$$
$$\nabla_n\cdot\mathbf{A} = 0, \tag{42}$$
$$\hat{n}\times\nabla\times\mathbf{F} = 0, \tag{43}$$
$$\hat{n}\cdot\mathbf{F} = 0. \tag{44}$$

and then the potential Green's functions for the internal region are given by

$$G_\phi^{int} = \frac{1}{\epsilon}G_d, \tag{45}$$
$$G_{A_{xx}}^{int} = \mu_0 G_d, \tag{46}$$
$$G_{A_{yy}}^{int} = \mu_0 G_d, \tag{47}$$
$$G_{A_{xz}}^{int} = \mu_0 G_n, \tag{48}$$
$$G_{A_{yz}}^{int} = \mu_0 G_n, \tag{49}$$
$$G_\psi^{int} = \frac{1}{\mu_0}G_n, \tag{50}$$
$$G_{F_{xx}}^{int} = -\epsilon G_n, \tag{51}$$
$$G_{F_{yy}}^{int} = -\epsilon G_n. \tag{52}$$

Using both modal and image representation, accelerated Green's function series are obtained [21]

$$\begin{aligned} G_d\left(\mathbf{r},\mathbf{r}'\right) \;&=\; {g_d}^{(m)} + \frac{1}{4\pi}\sum_{n=-\infty}^{\infty}\left(\frac{e^{-jkR_n{}^+}}{R_n{}^+} - \frac{e^{-jkP_n{}^+}}{P_n{}^+}\right.\\ &\left. -\frac{e^{-jkR_n{}^-}}{R_n{}^-} + \frac{e^{-jkP_n{}^-}}{P_n{}^-}\right) \end{aligned} \tag{53}$$

$$\begin{aligned} G_n\left(\mathbf{r},\mathbf{r}'\right) \;&=\; {g_n}^{(m)} + \frac{1}{4\pi}\sum_{n=-\infty}^{\infty}\left(\frac{e^{-jkR_n{}^+}}{R_n{}^+} - \frac{e^{-jkP_n{}^+}}{P_n{}^+}\right.\\ &\left. +\frac{e^{-jkR_n{}^-}}{R_n{}^-} - \frac{e^{-jkP_n{}^-}}{P_n{}^-}\right) \end{aligned} \tag{54}$$

where

$$\begin{aligned} {g_d}^{(m)}\left(\mathbf{r},\mathbf{r}'\right) \;&=\; \frac{1}{2\pi h}\sum_{n=1}^{\infty}\sin\left(\frac{n\pi}{2h}(z+h)\right)\\ &\times\sin\left(\frac{n\pi}{2h}(z'+h)\right)K_0(\alpha_n\rho_c) \end{aligned} \tag{55}$$

and

$${g_n}^{(m)}\left(\mathbf{r},\mathbf{r}'\right) \;=\; -\frac{j}{8h}{H_0}^{(2)}(k\rho_c) + \frac{1}{2\pi h}\sum_{n=1}^{\infty} \tag{56}$$

$$cos(\frac{n\pi}{2h}(z+h))$$

$$\times\cos(\frac{n\pi}{2h}(z'+h))K_0(\alpha_n\rho_c) \tag{57}$$

The derivatives of the Green's functions with respect to the vertical axis z are

$$\begin{aligned} \frac{\partial G_d\left(\mathbf{r},\mathbf{r}'\right)}{\partial z} \;&=\; \frac{\partial g_d^{(m)}}{\partial z}\left(\mathbf{r},\mathbf{r}'\right)\\ &+\frac{1}{4\pi}\sum_{n=-\infty}^{\infty}\Bigg\{\left(z-z'-4nh\right)\\ &\times\Bigg[e^{-jkP_n{}^+}\left(\frac{jk}{P_n^{+2}} + \frac{1}{P_n^{+3}}\right) \end{aligned}$$

$$
\begin{aligned}
&-e^{-jkR_n{}^{+}}\left(\frac{jk}{R_n^{+2}}+\frac{1}{R_n^{+3}}\right)\Bigg]\\
&+\left[z-z'-(2n+1)\,2h\right]\\
&\times\left[e^{-jkR_n{}^{-}}\left(\frac{jk}{R_n^{-2}}+\frac{1}{R_n^{-3}}\right)\right.\\
&\left.-e^{-jkP_n{}^{-}}\left(\frac{jk}{P_n^{-2}}+\frac{1}{P_n^{-3}}\right)\right]\Bigg\}
\end{aligned} \tag{58}
$$

$$
\begin{aligned}
\frac{\partial G_n\left(\mathbf{r},\mathbf{r}'\right)}{\partial z} &= \frac{\partial g_n^{(m)}}{\partial z}\left(\mathbf{r},\mathbf{r}'\right)\\
&+\frac{1}{4\pi}\sum_{n=-\infty}^{\infty}\Bigg\{\left(z-z'-4nh\right)\\
&\times\left[e^{-jkP_n{}^{+}}\left(\frac{jk}{P_n^{+2}}+\frac{1}{P_n^{+3}}\right)\right.\\
&\left.-e^{-jkR_n{}^{+}}\left(\frac{jk}{R_n^{+2}}+\frac{1}{R_n^{+3}}\right)\right]\\
&+\left[z-z'-(2n+1)\,2h\right]\\
&\times\left[e^{-jkP_n{}^{-}}\left(\frac{jk}{P_n^{-2}}+\frac{1}{P_n^{-3}}\right)\right.\\
&\left.-e^{-jkR_n{}^{-}}\left(\frac{jk}{R_n^{-2}}+\frac{1}{R_n^{-3}}\right)\right]\Bigg\}
\end{aligned} \tag{59}
$$

where

$$
\begin{aligned}
\frac{\partial g_d{}^{(m)}\left(\mathbf{r},\mathbf{r}'\right)}{\partial z} &= \frac{1}{4h^2}\sum_{n=1}^{\infty}n\ \cos(\frac{n\pi}{2h}(z+h))\\
&\times\sin\left(\frac{n\pi}{2h}(z'+h))K_0(\alpha_n\rho_c\right)
\end{aligned} \tag{60}
$$

and

$$
\begin{aligned}
\frac{\partial g_n{}^{(m)}\left(\mathbf{r},\mathbf{r}'\right)}{\partial z} &= -\frac{1}{4h^2}\sum_{n=1}^{\infty}n\ \sin\left(\frac{n\pi}{2h}(z+h)\right)\\
&\times\cos\left(\frac{n\pi}{2h}(z'+h))K_0(\alpha_n\rho_c\right)
\end{aligned} \tag{61}
$$

Here

$$\rho_0 = \sqrt{\left(x-x'\right)^2+\left(y-y'\right)^2}, \tag{62}$$

$$\rho_c = \sqrt{\rho_0{}^2+c^2}, \tag{63}$$

$$\alpha_n = \sqrt{\left(\frac{n\pi}{2h}\right)^2-k^2}, \tag{64}$$

$$R_n{}^{+} = \sqrt{\rho_0{}^2+\left(z-z'-4nh\right)^2}, \tag{65}$$

$$R_n{}^{-} = \sqrt{\rho_0{}^2+\left[z-z'-(2n+1)2h\right]^2}, \tag{66}$$

$$P_n{}^{+} = \sqrt{\rho_c{}^2+\left(z-z'-4nh\right)^2}, \tag{67}$$

$$P_n{}^{-} = \sqrt{\rho_c{}^2+\left[z-z'-(2n+1)2h\right]^2} \tag{68}$$

K_0 is the modified Bessel function of order 0 and $c \geq 0$.

B. External Region Green's Functions

For the external region the Green's function are the well known solutions for half space boundary conditions:

$$G_{\psi}^{ext} = \frac{1}{4\pi\mu_0}\frac{e^{-jk_0 r}}{r}, \tag{69}$$

$$G_{F_{xx}}^{ext} = G_{F_{yy}}^{ext} = -\frac{\epsilon_0}{4\pi}\frac{e^{-jk_0}}{r}. \tag{70}$$

Mostafa N. Abdulla (S'97–M'00) was born in Cairo, Egypt, in February 1970. He received the B.Sc. (with honors) and M.Sc. degrees from Ain Shams University, Cairo, Egypt in 1992 and 1996, respectively, both in electronics and communication engineering, and the Ph.D. degree in electrical engineering from North Carolina State University, Raleigh,in 1999. From 1992 to 1996, he was a Lecturer and Research Assistant in the Department of Electronics and Communication Engineering , Ain Shams University, where his research dealt with antennas and microwave circuits. From 1997 to 1999 he was with North Carolina State University, as a Research Assistant in Electronics Research Laboratory, Department of Electrical and Computer Engineering, where he performed research in electromagnetic modeling of active antennas and spatial power combining systems. In 1999, he was with Yazaki North America Inc., Canton, MI, as a Senior RF Engineer. Since 2000, he has been with Intel Corp., Sacramento, CA, as a Senior Engineer. His current interest include mixed signal design methodology and RF circuit design. Dr. Abdulla is a member of Phi Kappa Phi, IEEE Antennas and propagation, and IEEE Microwave Theory and Techniques Societies.

Michael Steer (S'76–M'78–SM'90–F'99) received his B.E. and Ph.D. in Electrical Engineering from the University of Queensland, Brisbane, Australia, in 1978 and 1983 respectively. Currently he is Professor of Electrical and Computer Engineering at North Carolina State University. In 1999 and 2000 he was Professor in the School of Electronic and Electrical Engineering at the University of Leeds where he still holds the Chair in Microwave and Millimeterwave Electronics. He was also Director of the Institute of Microwaves and Photonics at the University of Leeds. His research work has been closely tied to solving fundamental problems in modelling and implementing RF and microwave circuits and systems. His teaching and research interests are in global modelling of the physical layer of RF, microwave and millimeterwave electronic systems. Specific work is also directed at RF and microwave design; linearization of efficient power amplifiers; spatial power combining systems; design of millimetre-wave and terahertz frequency communication and imaging systems; and high efficiency low cost RF technologies for wireless applications. Professor Steer is an IEEE Fellow and is active in the Microwave Theory and Techniques (MTT) Society. In 1997 he was Secretary of the Society and was an Elected Member of the Administrative Committee from 1998 to 2000. He has organised many workshops and taught many short courses on Signal Integrity, Wireless, and RF Design. He has authored or co-authored more than 175 refereed papers and book chapters, including approximately 60 journal papers, on topics related to RF, microwave, and high-speed digital design methodology. He has one patent and has co-authored one book.